Charge Transport in Organic Crystals: Role of Disorder and Topological Connectivity

Thorsten Vehoff,[†] Björn Baumeier,*,[†] Alessandro Troisi,[‡] and Denis Andrienko*,[†]

Max Planck Institute for Polymer Research, Ackermannweg 10, D-55128 Mainz, Germany, and Department of Chemistry and Centre of Scientific Computing, University of Warwick, Coventry CV4 7AL, United Kingdom

Received May 20, 2010; E-mail: baumeier@mpip-mainz.mpg.de; denis.andrienko@mpip-mainz.mpg.de

Abstract: We analyze the relationship among the molecular structure, morphology, percolation network, and charge carrier mobility in four organic crystals: rubrene, indolo[2,3-*b*]carbazole with CH_3 side chains, and benzo[1,2-*b*:4,5-*b′*]bis[*b*]benzothiophene derivatives with and without C_4H_9 side chains. Morphologies are generated using an all-atom force field, while charge dynamics is simulated within the framework of high-temperature nonadiabatic Marcus theory or using semiclassical dynamics. We conclude that, on the length scales reachable by molecular dynamics simulations, the charge transport in bulk molecular crystals is mostly limited by the dynamic disorder, while in self-assembled monolayers the static disorder, which is due to the slow motion of the side chains, enhances charge localization and influences the transport dynamics. We find that the presence of disorder can either reduce or increase charge carrier mobility, depending on the dimensionality of the charge percolation network. The advantages of charge transporting materials with two- or three-dimensional networks are clearly shown.

1. Introduction

Among organic semiconducting materials, single crystals created by vapor deposition have record charge carrier mobilities.[1-4] A representative example is rubrene for which mobilities up to 15 cm²/(V s) have been reported.[5-7] As a result, performance of OFETs based on single crystals is comparable to that of amorphous silicon-based TFTs. Such devices, however, are of almost no use in practical applications. In contrast, thin-film-based OFETs,[8-11] while having many potential applications, have mobilities of active layers on the order of 1 cm²/(V s) only.

To assist the design of compounds suitable for thin organic layers, it would be helpful to understand what limits charge transport in self-assembled monolayers and, eventually, formulate design rules for organic semiconductors of this kind. This is a nontrivial task, since several factors can influence charge carrier mobility: (i) the molecular electronic structure, (ii) the relative positions of molecules in the crystal structure, and (iii) the disorder in the morphology arising from static or dynamic deviations from optimal single-crystal structures. In this situation, computer simulations can assist with the morphology characterization and can help to link electronic structure and morphology to charge mobility.[12] This is particularly challenging in the case of charge transport in organic materials, since even the type of transport can change depending on the degree of molecular ordering and temperature. For perfectly ordered defect-free crystals at low temperatures the Drude model based on band theory[5-7,13-21] or its extensions which account for local

---

† Max Planck Institute for Polymer Research.
‡ University of Warwick.

(1) Haemori, M.; Yamaguchi, J.; Yaginuma, S.; Itaka, K.; Koinuma, H. *Jpn. J. Appl. Phys.* **2005**, *44*, 3740–3742.
(2) Herwig, P. T.; Müllen, K. *Adv. Mater.* **1999**, *11* (6), 480–483.
(3) Murphy, A. R.; Fréchet, J. M. J.; Chang, P.; Lee, J.; Subramanian, V. *J. Am. Chem. Soc.* **2004**, *126* (6), 1596–1597.
(4) Kloc, C.; Tan, K.; Toh, M.; Zhang, K.; Xu, Y. *Appl. Phys. A: Mater. Sci. Process.* **2008**, *95* (1), 219–224.
(5) Ostroverkhova, O.; Cooke, D. G.; Hegmann, F. A.; Anthony, J. E.; Podzorov, V.; Gershenson, M. E.; Jurchescu, O. D.; Palstra, T. T. M. *Appl. Phys. Lett.* **2006**, *88* (16), 162101.
(6) Podzorov, V.; Menard, E.; Borissov, A.; Kiryukhin, V.; Rogers, J.; Gershenson, M. *Phys. Rev. Lett.* **2004**, *93* (8), 086602.
(7) Podzorov, V.; Menard, E.; Rogers, J. A.; Gershenson, M. E. *Phys. Rev. Lett.* **2005**, *95* (22), 226601.
(8) Takimiya, K.; Ebata, H.; Sakamoto, K.; Izawa, T.; Otsubo, T.; Kunugi, Y. *J. Am. Chem. Soc.* **2006**, *128* (39), 12604.
(9) Ebata, H.; Izawa, T.; Miyazaki, E.; Takimiya, K.; Ikeda, M.; Kuwabara, H.; Yui, T. *J. Am. Chem. Soc.* **2007**, *129* (51), 15732.
(10) Park, S. K.; Jackson, T. N.; Anthony, J. E.; Mourey, D. A. *Appl. Phys. Lett.* **2007**, *91* (6), 063514.
(11) Tsao, H. N.; Cho, D.; Andreasen, J. W.; Rouhanipour, A.; Breiby, D. W.; Pisula, W.; Müllen, K. *Adv. Mater.* **2009**, *21* (2), 209–212.

(12) Feng, X.; Marcon, V.; Pisula, W.; Hansen, M. R.; Kirkpatrick, J.; Grozema, F.; Andrienko, D.; Kremer, K.; Müllen, K. *Nat. Mater.* **2009**, *8*, 421.
(13) Glaeser, R. M.; Berry, R. S. *J. Chem. Phys.* **1966**, *44* (10), 3797.
(14) Silinish, E., Capek, V., Eds. *Organic Molecular Crystals: Interaction, Localization and Transport Phenomena*; American Institute of Physics: New York, 1994.
(15) Hutchison, G. R.; Zhao, Y.-J.; Delley, B.; Freeman, A. J.; Ratner, M. A.; Marks, T. J. *Phys. Rev. B* **2003**, *68* (3), 035204.
(16) Kim, E.-G.; Coropceanu, V.; Gruhn, N.; Sánchez-Carrera, R.; Snoeberger, R.; Matzger, A.; Brédas, J.-L. *J. Am. Chem. Soc.* **2007**, *129* (43), 13072.
(17) Troisi, A.; Orlandi, G. *J. Phys. Chem. B* **2005**, *109* (5), 1849.
(18) Jurchescu, O. D.; Baas, J.; Palstra, T. T. M. *Appl. Phys. Lett.* **2004**, *84* (16), 3061.
(19) Doi, K.; Yoshida, K.; Nakano, H.; Tachibana, A.; Tanabe, T.; Kojima, Y.; Okazaki, K. *J. Appl. Phys.* **2005**, *98* (11), 113709.
(20) Cheng, Y.; Silbey, R.; da Silva, D.; Calbert, J.; Cornil, J.; Bredas, J. *J. Chem. Phys.* **2003**, *118* (8), 3764.
(21) Yang, Y. T.; Yang, Y. M.; Wu, F. G.; Wei, Z. G. *Solid State Commun.* **2008**, *148*, 559.

electron−phonon coupling[22−25] are often used. At ambient conditions, however, the thermal fluctuations of the transfer integral, i.e., the nonlocal electron−phonon coupling, are of the same order of magnitude as the average value of the electronic coupling and charge transport should be treated as diffusion limited by thermal disorder. This can be achieved using semiclassical dynamics based on a model Hamiltonian with interacting electronic and nuclear degrees of freedom.[26−30] If nuclear dynamics is much slower than the dynamics of charge carriers (and electronic coupling is weak), charge transport can be described by a Hamiltonian with static disorder based on the electronic density of states and on the hopping rates between localized states. In this case, Marcus theory can be used to evaluate charge transfer rates.[12,31−33] However, it is a priori not clear which method is most suitable for partially disordered organic semiconductors, in spite of their rather extensive use,[12,31,32,34−40] since it is not apparent how much and what type of disorder is present in the system.

In this paper, a combination of molecular dynamics and charge carrier dynamics simulations is used to analyze how charge transport properties depend on the morphology, type of disorder (static or dynamic), and directionality and dimensionality of the charge percolation network in organic crystals. To this end, connections between the morphology and the transfer integral distributions are established, and the mobility is calculated by using both semiclassical dynamics and a rate-based approach. As test systems, we consider four different organic crystals, the chemical structures of which are given in Figure 1: rubrene, indolo[2,3-*b*]carbazole with CH_3 side chains,[41] and benzo[1,2-*b*:4,5-*b'*]bis[*b*]benzothiophene (BBBT) derivatives with and without C_4H_9 side chains.[42] In contrast to highly purified rubrene single crystals, which are created by vapor

deposition, the structures of indolocarbazole and the BBBT derivatives are obtained by self-assembly after spin coating. The conjugated core of indolocarbazole is similar to pentacene, and the presence of a nitrogen in the core introduces a binding site, which may be used for the attachment of functional groups that allow variation of the solubility and tuning of the molecular arrangement. BBBT is a conjugated molecule with a rigid fused-ring structure similar to pentacene. A straightforward, high-yield synthesis of BBBT and its alkyl-substituted derivatives has recently been developed.[42]

The paper is organized as follows: In section 2 we briefly describe the methodology of our calculations, covering how we obtain the larger scale morphologies using molecular dynamics simulations, as well as the procedure to analyze the charge transfer properties. Section 3 summarizes the results of our simulations. We discuss the relation of the disorder and connectivity network of the respective compounds to the obtained charge carrier mobility.

2. Methodology

Here, we briefly summarize the procedures we use to study charge transport properties. Single-crystal structures based on X-ray data[41−43] (see the Supporting Information) are used as the starting point. To account for the effect of thermal molecular motion, we perform molecular dynamics (MD) simulations on suitably defined supercells. In the case of rubrene, these simulations were performed using Tinker[44] in combination with the MM3 force field[45] to have an exact reproduction of the reference situation in ref 28. For indolocarbazole and the two BBBT derivatives, we used the GROMACS package[46] with a force field based on OPLS parameters. Explicit details about force-field parameters and the MD simulations can be found in the Supporting Information. Density-functional theory (DFT) calculations were performed with the Gaussian03 package[47] to obtain reorganization energies for a single molecule in vacuum using the B3LYP hybrid functional[48] and a 6-311G(d,p) basis set. The calculations yield values of 0.159 eV for rubrene, 0.212 eV for indolocarbazole, and 0.120 eV for BBBT. Transfer integrals between neighboring molecules are evaluated using a method based on Zerner's intermediate neglect of differential overlap as implemented in the Molecular Orbital Overlap package.[49] Selected results have been checked against transfer integrals obtained from DFT-based calculations using the dimer projection method presented in ref 50. No significant differences could be observed.

The resulting total transfer integral distributions are then analyzed in terms of partial distributions associated with the orientation of neighbors within the respective crystal structures, i.e., its main transporting directions. To determine whether the width of the distributions is due to static (on the time scale of charge transport) disorder, i.e., caused by the irregular arrangement of the molecules, or dynamic disorder due to the motions/vibrations of the molecules, we compare the respective ensemble distributions to time distributions for selected molecular pairs. The time distributions are formed over 1000 snapshots taken every 20 fs.

(22) Munn, R. W.; Silbey, R. *J. Chem. Phys.* **1985**, *83* (4), 1843.
(23) Munn, R. W.; Silbey, R. *J. Chem. Phys.* **1985**, *83* (4), 1854.
(24) Hannewald, K.; Bobbert, P. A. *Phys. Rev. B* **2004**, *69* (7), 075212.
(25) Hannewald, K.; Bobbert, P. A. *Appl. Phys. Lett.* **2004**, *85* (9), 1535.
(26) Moorthy, J. N.; Venkatakrishnan, P.; Savitha, G.; Weiss, R. G. *Photochem. Photobiol. Sci.* **2006**, *5*, 903.
(27) Troisi, A.; Orlandi, G. *J. Phys. Chem.* **2006**, *110*, 4065–4070.
(28) Troisi, A. *Adv. Mater.* **2007**, *19* (15), 2000–2004.
(29) Cheung, D. L.; Troisi, A. *Phys. Chem. Chem. Phys.* **2008**, *10* (39), 5941.
(30) Troisi, A. *Organic Electronics*; Advances in Polymer Science; Springer: Berlin/Heidelberg, 2009.
(31) Kirkpatrick, J.; Marcon, V.; Nelson, J.; Kremer, K.; Andrienko, D. *Phys. Rev. Lett.* **2007**, *98*, 227402.
(32) Kwiatkowski, J. J.; Nelson, J.; Li, H.; Bredas, J. L.; Wenzel, W.; Lennartz, C. *Phys. Chem. Chem. Phys.* **2008**, *10*, 1852–1858.
(33) Marcon, V.; Kirkpatrick, J.; Pisula, W.; Andrienko, D. *Phys. Status Solidi B* **2008**, *245* (5), 820.
(34) Lemaur, V.; da Silva Filho, D. A.; Coropceanu, V.; Lehmann, M.; Geerts, Y.; Piris, J.; Debije, M. G.; van de Craats, A. M.; Senthilkumar, K.; Siebbeles, L. D. A.; Warman, J. M.; Bredas, J.-L.; Cornil, J. *J. Am. Chem. Soc.* **2004**, *126* (10), 3271.
(35) Nagata, Y.; Lennartz, C. *J. Chem. Phys.* **2008**, *129* (3), 034709.
(36) Andrienko, D.; Kirkpatrick, J.; Marcon, V.; Nelson, J.; Kremer, K. *Phys. Status Solidi B* **2008**, *245*, 830.
(37) Troisi, A.; Cheung, D. L.; Andrienko, D. *Phys. Rev. Lett.* **2009**, *102*, 116602.
(38) Marcon, V.; Pisula, W.; Dahl, J.; Breiby, D. W.; Kirkpatrick, J.; Patwardhan, S.; Grozema, F.; Andrienko, D. *J. Am. Chem. Soc.* **2009**, *131*, 11426–11432.
(39) Lukyanov, A.; Lennartz, C.; Andrienko, D. *Phys. Status Solidi A* **2009**, *206*, 2737–2742.
(40) Rühle, V.; Kirkpatrick, J.; Andrienko, D. *J. Chem. Phys.* **2010**, *132*, 134103.
(41) Wrobel, N. Synthese und Photophysikalische Eigenschaften von Indolocarbazolen und Höheren Analoga. Thesis, Johannes Gutenberg Universität Mainz, 2008.
(42) Gao, P.; Beckmann, D.; Tsao, H. N.; Feng, X.; Enkelmann, V.; Pisula, W.; Müllen, K. *Chem. Commun.* **2008**, 1548–1550.

(43) Jurchescu, O.; Meetsma, A.; Pastra, T. *Acta Crystallogr., B* **2006**, *62*, 330.
(44) Tinker 5.1, http://dasher.wustl.edu/tinker/.
(45) Allinger, N.; Yuh, Y.; Lii, J.-H. *J. Am. Chem. Soc.* **1989**, *111*, 8551.
(46) Hess, B.; Kutzner, C.; van der Spoel, D.; Lindahl, E. *J. Chem. Theory Comput.* **2008**, *4*, 435.
(47) Frisch, M. J.; et al. *Gaussian03*, revision C.02; Gaussian, Inc.: Wallingford, CT, 2004.
(48) Stevens, P. J.; Devlin, F. J.; Chabalowski, C. F.; Frisch, M. J. *J. Phys. Chem.* **1993**, *98*, 11623.
(49) Kirkpatrick, J. *Int. J. Quantum Chem.* **2008**, *108*, 51.
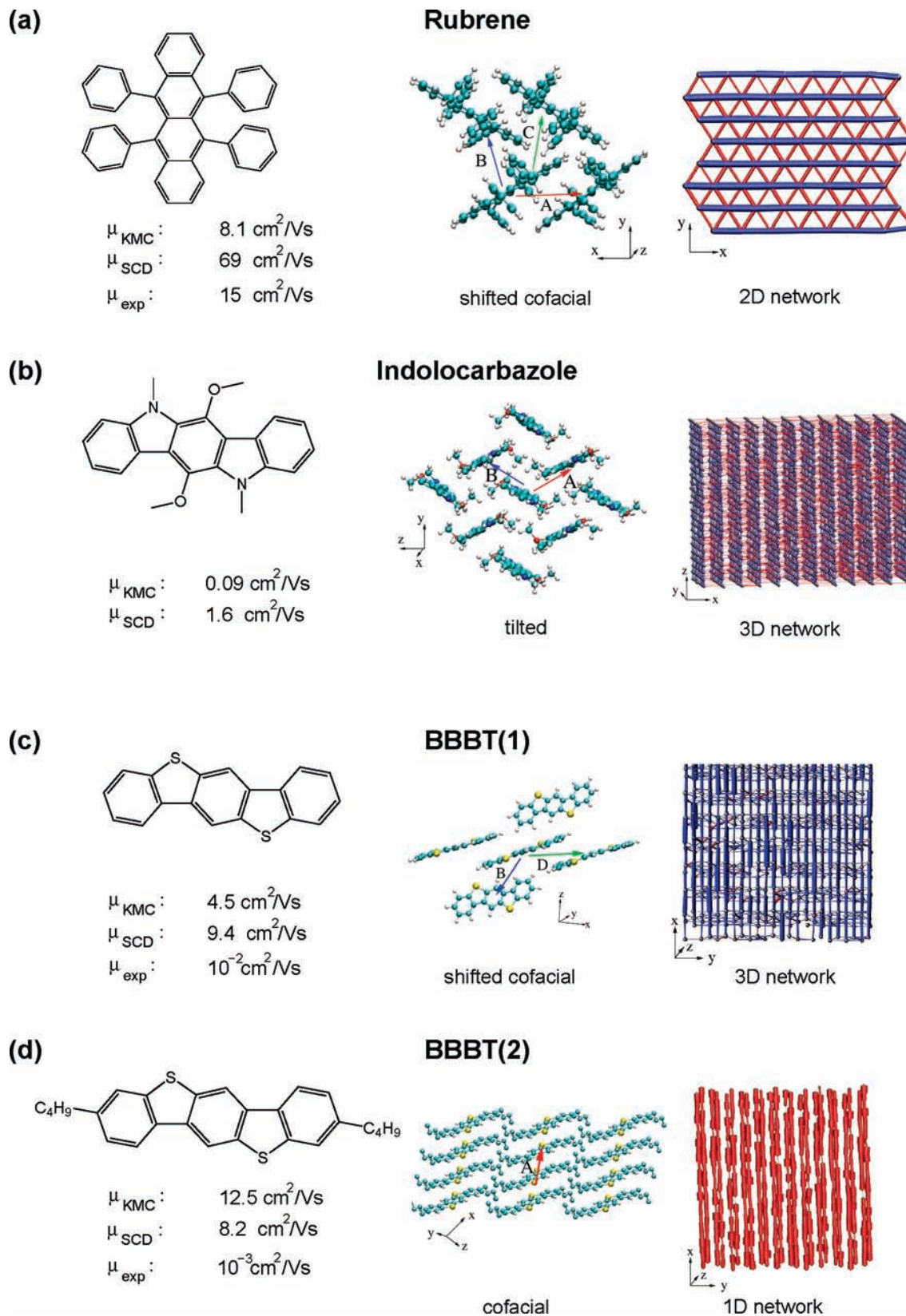(50) Baumeier, B.; Kirkpatrick, J.; Andrienko, D. *Phys. Chem. Chem. Phys.*, (DOI: 10.1039/C002337J).

Figure 1. Comparison of the nearest neighbor alignment along the main transport direction and the connectivity in the system for rubrene, indolocarbazole, and the two BBBT derivatives. Gray spheres in the connectivity graphs represent the centers of mass, while the size (color) of the bonds between them is proportional to the absolute value (sign) of the corresponding transfer integral. Experimental values for hole mobilities are taken from refs 5−7 and 55 (rubrene) and ref 42 (BBBT).

Connectivity graphs show the strength of the intermolecular coupling between lattice sites (centers of masses) based on the magnitude of the individual transfer integrals. These graphs are used to visualize the effect of disorder on the topology of the transporting network in the crystalline systems and to elucidate the dimensionality and directionality of the charge transport.

Finally, the hole mobility is determined using (a) kinetic Monte Carlo (KMC) simulations based on Marcus rates[51,52]

$$\omega_{ij} = \frac{J_{ij}^2}{\hbar} \sqrt{\frac{\pi}{\lambda k_B T}} \exp\left[-\frac{(\Delta G_{ij} - \lambda)^2}{4 k_B T \lambda}\right] \qquad (1)$$

where λ is the reorganization energy and ΔG_{ij} is the free energy difference between initial and final states and (b) one-dimensional semiclassical dynamics for directions in which the transfer integral distributions indicate strong electronic coupling. Morphology analysis and KMC simulations were done using the VOTCA package.[53]

In case (a), the free energy difference ΔG_{ij} in the exponent of the Marcus rates (eq 1) needs to be evaluated. Several factors contribute to ΔG_{ij} such as electrostatic interactions and interaction with the externally applied electric field. We calculated the dipole moment for the optimized geometries of a single molecule in vacuum using B3LYP/6-311G(d,p), yielding 0.0474 D (though it depends on the conformation of the side chains) for rubrene, while it is zero for indolocarbazole and BBBT due to the molecular symmetry. We therefore neglect the contribution to energetic disorder arising from electrostatic interactions. Note, however, that quadrupoles or higher order multipoles can also contribute to energetic disorder.[54] Thus, in the following, we set $\Delta G_{ij} = e E r_{ij}$, where e is the elementary charge, r_{ij} is the vector connecting molecules i and j, and $E = 10^7$ V/m is the magnitude of the externally applied electric field. Charge carrier mobilities in the three spatial directions are based on velocity averaging runs over multiple snapshots and different starting positions. For each direction, the external electric field is aligned parallel to it.

In the case of the semiclassical dynamics (b), a one-dimensional array of molecules is chosen such that it corresponds to the respective direction of strong coupling within the crystal. The separation between the sites d equals the average distance between nearest neighbors of that type. The average transfer integral between sites is the configurational (ensemble) average along that particular direction, and the standard deviation is equal to the width of the $J(t)$ distribution for neighboring pairs with a similar average. This ensures that we take into account only dynamic and not static disorder. The discrete cosine transform of the autocorrelation of $J(t)$ is averaged over five to seven different pairs to yield the characteristic slow vibrational frequency $\omega^{(2)}$ in the system. The fast vibrational frequency $\omega^{(1)}$ is chosen to be that of C−C bond fluctuations in phenyl rings and is thus the same for all systems (see again ref 28). The Peierls and Holstein coupling constants were calculated using the reorganization energies mentioned above. The resulting input parameters used in the SCD simulations for all systems are summarized in the Supporting Information. All simulations were run at 300 K, the integration time step was chosen to be 0.0125 fs, and each simulation consists of 600 000 steps. The simulations are repeated for 100 starting wave functions, and the resulting random mean square displacement is Boltzmann averaged using the energy eigenvalue of the initial wave function for the weighting.

3. Results

Figure 1 summarizes the results of our analysis of morphology, connectivity, and charge carrier mobilities in crystalline phases of rubrene, indolocarbazole, and the two BBBT derivatives. We will refer to it in the following subsections.

(51) Marcus, R. A. *Rev. Mod. Phys.* **1993**, *65*, 599.
(52) Hutchison, G. R.; Ratner, M. A.; Marks, T. J. *J. Am. Chem. Soc.* **2005**, *127*, 2339.
(53) Rühle, V.; Junghans, C.; Lukyanov, A.; Kremer, K.; Andrienko, D. *J. Chem. Theory Comput.* **2009**, *5*, 3211–3223.
(54) Novikov, S. V. *Ann. Phys.* **2009**, *18*, 949.
(55) Sundar, V.; Zaumseil, J.; Podzorov, V.; Menard, E.; Willet, R.; Someya, T.; Gershenson, M.; Rogers, J. *Science* **2004**, *303*, 1644.
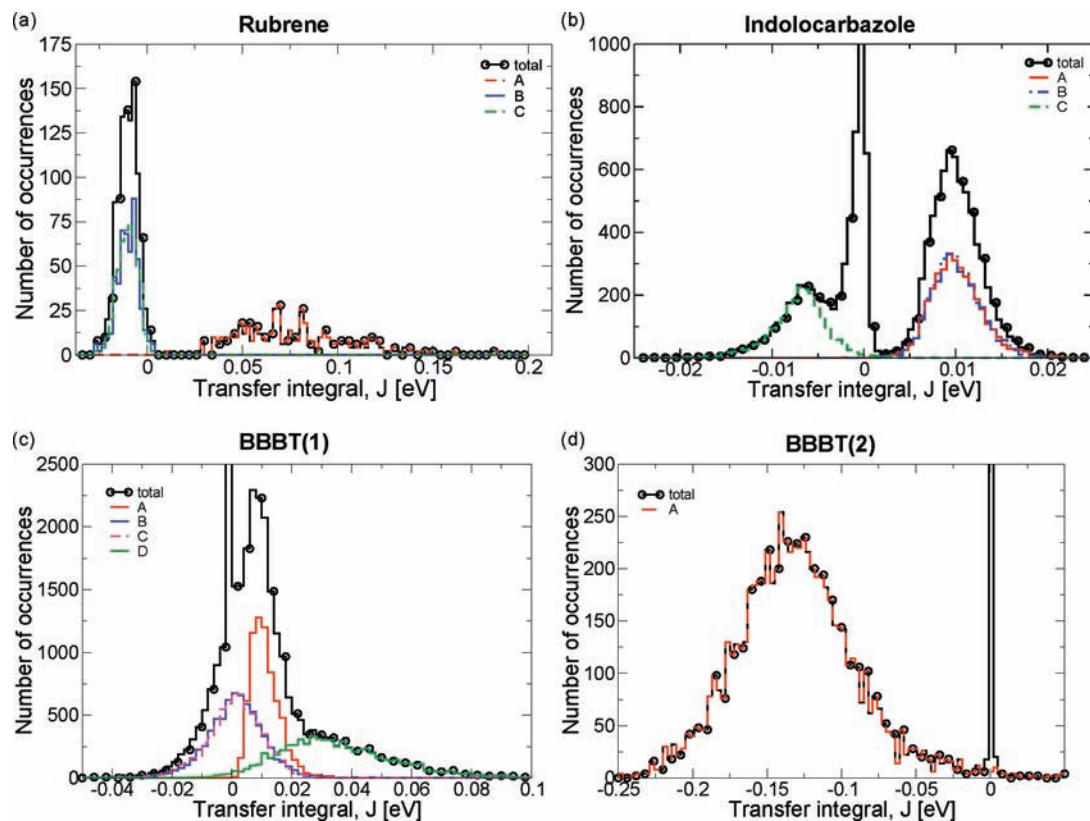
3.1. Transfer Integrals and Directionality. On the basis of the equilibrated structures obtained from the MD simulations, we first analyze the characteristics of the electronic coupling between neighboring molecules and relate features in the ensemble distributions to directions within the respective crystal structures. The total and direction-resolved distributions of transfer integrals for the four organic crystals are shown in Figure 2. The respective directions are defined in Figure 1.

In the case of rubrene, Figure 2a, there is no electronic coupling along the z direction since the centers of mass of the molecules are diagonally displaced by about 1.4 nm, and the distance of closest approach is between the hydrogens of the side chain phenyls. In contrast, within the same xy plane, there are three different major directions of electronic coupling, which are labeled A, B, and C as in Figure 1a. It can be seen that the total distribution can be decomposed in terms of the three respective direction-resolved ones. Along the A direction the neighbors are cofacially oriented and on average shifted by 0.714 nm with respect to each other along the x axis. The average coupling for this direction is very high but has a broad distribution, $J_A = 0.078 \pm 0.030$ eV. In directions B and C neighboring molecules are tilted with respect to each other so that there is no cofacial alignment between them, and consequently, the electronic coupling is lower. Both partial distributions exhibit a pronounced peak at $J_B = J_C = -0.010 \pm 0.006$ eV. For all directions the case of zero coupling between neighbors is at the very edge of the distributions, and thus, all molecules in the xy plane are coupled.

In indolocarbazole, one can also identify three different types of neighboring pairs in the crystal, which are labeled A, B, and C in Figure 1b. Neighbors of types A and B lie in the yz plane with the centers of mass of the molecules separated by 0.639 nm. The transfer integral distributions for A and B in a single snapshot are shown by the red and blue curves in Figure 2b and are similar, with $J_A = J_B = 0.010 \pm 0.003$ eV on the basis of averaging over respective pairs in a single snapshot. Neighbors of type C are displaced by 1.111 nm along the x direction. The minimal distance between them is much smaller and enables transport along the x direction. The corresponding transfer integral distribution is centered at $J_C = -0.006 \pm 0.003$ eV. The large additional peak at zero in the total transfer integral distribution is due to second-order neighbors, which are removed prior to the KMC runs.

In the crystal structure of BBBT(1) there are four types of neighboring pairs $A-D$ between which charge transport can occur (see Figures 1c and 2c). The three types of pairs A, B, and C contribute mainly to transport in the yz plane. In particular, A has the lowest center of mass distance of 0.587 nm along the y direction. The molecules are in strongly tilted cofacial alignment, leading to an average transfer integral of $J_A = 0.011 \pm 0.004$ eV. Neighbors of types B and C are at an identical distance of 0.735 nm. Despite the proximity of the neighbors, the tilt of the molecules in opposite directions with the cores almost perpendicular to each other leads to little overlap between orbitals, resulting in a weak electronic coupling of $J_B = J_C = 0.001 \pm 0.009$ eV. The strongest electronic coupling is found along the x axis in direction D, where neighbors are displaced by 0.926 nm relative to each other, due to a shifted cofacial alignment. The corresponding transfer integral distribution has a fairly high average value but is also very broad with $J_D = 0.036 \pm 0.020$ eV. As for indolocarbazole, the peak at zero in the transfer integral distribution of the entire system is explained by second-order neighbors.

Figure 2. Total (black) and direction-resolved (see Figure 1 for definitions) distributions of transfer integrals in the four organic crystals studied in this work.

Attachment of alkyl side chains changes the crystal structure of BBBT(1) into one with a significantly different ordering of neighbors. BBBT(2) aligns in a stacked columnar phase, where each molecule has only two close neighbors. The molecules have practically perfect cofacial alignment along the column as illustrated in Figure 1d. The total transfer integral distribution splits into two parts, as shown in Figure 2d: the distribution due to neighbors along the *A* direction and a peak at zero, which contains the contributions of all neighbors in directions other than *A*. The interplanar separation of the lamellar structure is only 0.342 nm, which leads to a strong electronic coupling of $J_A = -0.130 \pm 0.042$ eV. Notably, this value exceeds even the one along rubrene's main coupling direction. However, unlike in the case of rubrene, no significant coupling in perpendicular directions is registered due to the presence of the side chains and the alignment of the molecules in isolating neighboring stacks. Neighbors perpendicular to the stacking direction can only interact via the side hydrogens, resulting in low transfer integrals with maximum values on the order of 10^{-3} eV. The presence of the side chains thus effectively renders BBBT(2) a one-dimensional semiconductor, in which transport can only be expected along the stacking direction *A* of the columns.

3.2. Analysis of the Type of Disorder. As mentioned in section 2, a comparison of the time distribution of transfer integrals $\langle J(t) \rangle$ for selected neighbor pairs with the respective ensemble distributions J_{conf} can help to identify whether the observed disorder is of static or dynamic nature. In the following, we select neighbor pairs that belong to the direction of strongest coupling as determined above, i.e., direction *A* for rubrene, indolocarbazole, and BBBT(2) and direction *D* for BBBT(1). The comparison (a figure is included in the Supporting Information) shows that in rubrene, indolocarbazole, and

BBBT(1) the width of each of the time distributions is similar to that of the configurational distribution. This means that thermal fluctuations between neighbors lead to variations in transfer integrals which are of the same magnitude as variations throughout the system. This indicates that static disorder is small and that transfer integral fluctuations are mainly due to thermal fluctuations. In contrast, the time distributions of transfer integrals in direction *A* in BBBT(2) are significantly different from the configurational distribution. This indicates the presence of static disorder along the column, which may be explained by the slow motions of the soft side chains and resulting displacements of the molecules in the direction of their long axis.[56]

3.3. Connectivity Graphs. Connectivity graphs computed for a single representative snapshot, as shown in Figure 1, reveal characteristic features of the charge percolation network. In all cases, gray spheres represent the centers of mass of the molecules, and the thickness of the bonds between them corresponds to the magnitude of the connecting transfer integral and color to the sign, with red being negative and blue positive. No bonds are drawn in cases where the absolute value of the transfer integral between neighbors is below 0.005 eV. As we already pointed out when analyzing the transfer integral distributions in Figure 2, rubrene exhibits electronic coupling only between molecules residing in the same *xy* plane. The respective connectivity graph in Figure 1 shows no defects throughout, and the sign of the transfer integrals is always identical in a given direction; i.e., molecular vibrations are not strong enough to lead to a complete loss of coupling between

(56) Vehoff, T.; Chung, Y.; Johnston, K.; Troisi, A.; Yoon, D. Y.; Andrienko, D. *J. Phys. Chem. C* **2010**, *114*, 10592.

Table 1. Hole Mobilities [cm²/(V s)] for Rubrene, Indolocarbazole, and BBBT without and with C_4H_9 Side Chains[a]

	KMC				
	x	*y*	*z*	SCD	FET
rubrene	8.14	0.45	3×10^{-8}	69.3	15[b]
indolocarbazole	0.09	0.06	0.09	1.57	
BBBT(1)	4.53	0.33	0.30	9.43	10^{-2} [c]
BBBT(2)	12.51	10^{-4}	4×10^{-8}	8.15	10^{-3} [c]

[a] Experimental field-effect transistor data are given for rubrene and BBBT, although no direction of transport was specified in the respective papers. [b] From refs 5−7 and 55. [c] From ref 42.

neighboring molecules. Rubrene thus features a two-dimensional defect-free charge carrier percolation network.

Since the transfer integrals for indolocarbazole are about 1 order of magnitude smaller than in rubrene's main transport direction, the bonds drawn in Figure 1b are thinner, in general. This difference can be explained by the CH_3 and OCH_3 side chains, which prevent a close approach of the conjugated cores of neighboring molecules. However, the resulting absolute values of the transfer integrals are of the same order as those obtained for the weaker coupling in directions *B* and *C* in rubrene. The transfer integral distributions alone do not reveal a preferred transport direction, although electronic coupling in the *C* and thus the *x* direction is almost a factor of 2 lower than in the *A* and *B* directions. Consequently, the connectivity network in Figure 1b shows only a very few defects and hence plenty of possible percolation pathways in the *yz* plane. Within the *xz* plane, however, one registers a number of disruptions in connectivity due to the lower coupling in the *C* direction. Still, this does not render charge transport unlikely. Indolocarbazole can thus be regarded as an almost isotropic 3D transporting compound. Combined with the little static disorder in the system, this results in a well-connected charge carrier percolation network spanning all three spatial dimensions.

In the case of BBBT(1), the connectivity graph as shown in Figure 1c gives a clear indication of strong transport along the *x* axis with weaker interconnections in the *yz* plane. Therefore, as one might expect due to the lack of side chains, BBBT(1) exhibits the characteristics of a three-dimensional semiconductor. Contrary to indolocarbazole, however, the 3D network of BBBT(1) possesses a strongly preferred transport direction.

BBBT(2), in contrast, shows connectivity only along the *x* direction (see Figure 1d). As indicated by the width of the bonds in the connectivity graph, the electronic coupling between most neighbors is very strong. Notable exceptions are single cases, in which the coupling is significantly weaker. Due to the one-dimensional percolation network, these weak couplings have significant impact on the charge transport in BBBT(2), since unlike in BBBT(1) charge carriers cannot circumvent defects.

3.4. Mobility Calculations. Table 1 summarizes calculated hole mobilities that are obtained by velocity averaging of KMC simulations based on Marcus rates, one-dimensional semiclassical dynamics calculations, and experimental FET measurements.

In general, the results from the rate-based KMC approach reflect the directionality that has been observed in the connectivity graphs. Rubrene shows a high mobility of 8.14 cm²/(V s) in the *x* direction, which corresponds to direction *A* defined in Figure 1a. Perpendicular, in the *y* direction, the mobility is 0.45 cm²/(V s), while it is only 3×10^{-8} cm²/(V s) in the *z* direction. This underlines the notion that rubrene is a compound with 2D transporting characteristics with the highest mobility along the direction of shifted cofacially aligned molecules.

Quantitatively, however, the mobility even along the *x* axis is lower than the one experimentally measured in OFETs[5−7,55] (15 cm²/(V s)), although it is of the same order of magnitude. The fact that the average transfer integral in the *A* direction (J_A = 0.078 eV) is comparable to the reorganization energy (λ = 0.159 eV) indicates that the assumption of a fully site localized charge as described in the hopping regime may not be fully valid in this direction. Instead, the charge is likely to be spread over several sites, and the small polaron regime as treated within the diffusion limited by thermal disorder model using semiclassical dynamics should be considered. Such simulations predict a mobility of 69 cm²/(V s) for rubrene, which is significantly higher than the rate-based value. It also exceeds the experimental OFET mobility. Since static disorder is not significant in rubrene and since there are no low rates in the *A* direction, we believe that the one-dimensionality of SCD does not neglect important system properties and thus SCD provides the upper limit of the mobility, which may be achieved in a perfect crystal.

As mentioned before, the connectivity graph of indolocarbazole, Figure 1b, shows characteristics of a 3D transporting network. Accordingly, rate-based simulations yield mobilities of approximately 0.09 cm²/(V s) in both the *x* and *y* directions and 0.06 cm²/(V s) in the *z* direction, showing hardly any spatial preference. Quantitatively, the maximum mobility is almost 2 orders of magnitude lower than that of rubrene in its main transport direction, but only less than 1 order of magnitude below the one in rubrene's *y* direction. Taking into account the weaker transfer integrals and the higher reorganization energy of indolocarbazole, this is a result of its almost defect free 3D charge percolation network. SCD simulations predict a mobility of 1.7 cm²/(V s), which is again more than 1 order of magnitude below that of rubrene, but still surprisingly high, since the isotropic percolation network does not positively influence the one-dimensional SCD simulations. The narrow width of the transfer integral distributions may be responsible for this.

In BBBT(1), kinetic Monte Carlo simulations predict a mobility of 4.5 cm²/(V s) in the *x* direction, 0.33 cm²/(V s) in the *y* direction, and 0.29 cm²/(V s) in the *z* direction. It is similar to rubrene, especially since molecules are also in shifted cofacial alignment along its main transport direction. While the mobility is predicted to be slightly weaker in both the *x* and *y* directions compared to that of rubrene, BBBT(1) exhibits significant mobility in the *z* direction as well. It is therefore a truly 3D transporting system.

For BBBT(2), KMC runs yield a mobility of 12.5 cm²/(V s) along the *x* axis, which exceeds even that of rubrene. This is not surprising, since the mean of the distribution of transfer integrals in that direction is higher and the reorganization energy is lower. However, transport along all other directions is negligible, i.e., $\sim 10^{-4}$ and $\sim 10^{-8}$ cm²/(V s) in the *y* and *z* directions, respectively. BBBT(2) is thus a 1D transporting compound. As such, its mobility will also depend on the tail of the transfer integral distribution as a single low transfer integral will reduce charge transport within a column.

When charge transport is treated using semiclassical dynamics, the mobility along the main transport directions of BBBT(1) and BBBT(2) is predicted to be 9.43 and 8.15 cm²/(V s), respectively. The fact that BBBT(1) actually shows slightly higher mobility than BBBT(2) is explained by the fact that the lower coupling in BBBT(1) is partially compensated by the larger distance of 0.93 nm a charge travels between neighboring molecules in the shifted cofacial direction of BBBT(1) while it travels only 0.47 nm in BBBT(2). In addition, the Peierls

coupling constant for BBBT(1) is also only a quarter of that of BBBT(2), since the molecules have lower weight and the transfer integral distributions are more narrow.

Summarizing, we find from our simulations that rubrene and the BBBT compounds all show very high mobilities along the directions of their strongest coupling, i.e., along the *A* direction in the case of rubrene and BBBT(2) and along the *D* direction in BBBT(1), where neighboring molecules are in either cofacial or shifted cofacial alignment. The mobility in indolocarbazole is almost 2 orders of magnitude lower, but with equally good transport in all three dimensions. BBBT(1) is also 3D transporting. However, the *y* and *z* directions are 1 order of magnitude weaker than the *x* direction. Rubrene is a 2D transporting material, also with an order of magnitude stronger transport along the *x* than along the *y* axis. BBBT(2) shows no transport perpendicular to the main direction.

3.5. Discussion and Conclusions. We first compare our simulation results to the experimentally available data. Simulations (see Figure 1 and Table 1) predict that, except for rubrene, both KMC and SCD tend to overestimate the value of mobility by 3−4 orders of magnitude. A rather good agreement for rubrene implies that the various approximations, for instance those regarding the validity of Marcus theory or the use of semiempirical methods for transfer integral calculations, cannot be the only reasons for such discrepancies.

Due to short simulation times and small system sizes, grain boundaries and defects cannot be accounted for in our simulations. We can therefore assume that the transport in real films is defect-limited. Since the influence of defects on mobility is more pronounced in 1D conductors than in 2D or 3D ones, we can justify this assumption by correlating the topology of the percolating network to the error we make when predicting the mobility.

Indeed, rubrene has a two-dimensional percolation network, featuring a clearly preferred transport direction with an extremely high coupling and a good secondary direction allowing the charge carrier to circumvent possible defects. In addition, rubrene single crystals are made by vapor deposition,[1] and rubrene's purity is extremely high.[4] Therefore, disorder in realistic rubrene layers is expected to be substantially smaller and closer to the situation covered by our simulations than in other crystals studied here. Hence, the agreement between measured and predicted mobilities is adequate.

BBBT(1) has a percolation network similar to that of rubrene with slightly worse coupling along its main and secondary directions, which eventually yields a lower overall mobility. The additional percolation paths gained by going from the 2D to 3D network do not influence the value of mobility strongly because the basic existence of pathways to circumvent neighbors with low transfer integrals is more important than their number. In this case, both SCD and KMC overestimate the mobility by 2 orders of magnitude.

BBBT(2) transports only in one direction. The influence of neighbors with low coupling therefore is substantially higher since the mobility is limited by the lowest rate present in a column. Hence, the effect of defects will be significantly more pronounced here than in BBBT(1). Indeed, even though SCD and KMC predict mobility values similar to those of BBBT(1), we overestimate the experimental value by almost 4 orders of magnitude.

Another indirect indication of the defect-dominated transport is that in our simulations the value of mobility can vary by a few orders of magnitude depending on the transport direction (see Table 1). Such variation is rarely observed or reported in experimental measurements.[42]

Summarizing, we can conclude that our estimates provide the upper limit of mobilities which can be achieved in perfectly aligned crystals or self-assembled monolayers. To account for large-scale defects, significantly larger samples would be required, which is beyond the current capabilities of MD simulations. Additionally, chemical defects and inhomogeneities of the gate electrodes likely contribute to the experimentally determined mobilities.

On the basis of the simulation results, we can also formulate several compound design rules for achieving high mobilities in well-aligned crystals. First, the general concept that the best coupling and thus the best transport properties will be found for closely packed, cofacially aligned molecules should be reconsidered. Certainly, the transfer integral is at its absolute maximum for two molecules in cofacial alignment about 3.5 nm apart, and therefore, the mobility along this direction is also at its maximum. However, the resulting morphology is likely to allow only one-dimensional transport and thereby becomes extremely prone to defects. Instead, shifted cofacial alignment, as is found for BBBT(1) and rubrene, is the better alternative. While the transfer integrals will be lower due to smaller spatial overlap between molecules, the distance traveled by a charge upon moving from one molecule to the other is increased, compensating for most of the loss in coupling. Most importantly, the shifted alignment allows two-dimensional transport and reduces the influence of defects. An immediate implication is that, for molecules with a linear conjugated core, attachment of the side chains perpendicular to the conjugated core, as is the case for rubrene, should result in morphologies with higher mobilities.

Supporting Information Available: Details of molecular dynamics simulations, force-field parameters, parameters used in semiclassical dynamics, and complete ref 47. This information is available free of charge via the Internet at http://pubs.acs.org.

JA104380C